

Connectivity precedes function in the development of the visual word form area

Zeynep M Saygin^{1,2}, David E Osher³, Elizabeth S Norton⁴, Deanna A Youssoufian⁵, Sara D Beach^{1,2}, Jenelle Feather¹, Nadine Gaab⁶, John D E Gabrieli^{1,2} & Nancy Kanwisher^{1,2}

What determines the cortical location at which a given functionally specific region will arise in development? We tested the hypothesis that functionally specific regions develop in their characteristic locations because of pre-existing differences in the extrinsic connectivity of that region to the rest of the brain. We exploited the visual word form area (VWFA) as a test case, scanning children with diffusion and functional imaging at age 5, before they learned to read, and at age 8, after they learned to read. We found the VWFA developed functionally in this interval and that its location in a particular child at age 8 could be predicted from that child's connectivity fingerprints (but not functional responses) at age 5. These results suggest that early connectivity instructs the functional development of the VWFA, possibly reflecting a general mechanism of cortical development.

The last two decades of neuroimaging research have revealed the functional organization of the human brain in unprecedented detail. Dozens of cortical regions have been identified, each with a distinctive functional profile and each found in approximately the same anatomical location in virtually every normal adult. How does this systematic functional organization arise in development? We asked specifically how a particular cortical location becomes earmarked as the future site at which a particular functionally specific region will develop.

A clue comes from previous findings in adults showing a close and fine-grained relationship between the functional response profile of each voxel in a region of cortex and the extrinsic connectivity of that voxel to the rest of the brain, measured with diffusion tractography in the same subject^{1,2}. This tight relationship between function and connectivity across the cortex suggests a developmental hypothesis: patterns of extrinsic connectivity (or connectivity fingerprints) may arise early in development, instructing subsequent functional development^{3,4}. Prior evidence for this hypothesis comes from classic studies in ferrets showing that, if retinal input is rerouted to medial geniculate nucleus (MGN) and subsequently primary auditory cortex (A1), A1 takes on many functional properties of V1 (refs. 5–9). However, it remains unclear whether similar mechanisms underlie the development of nonprimary cortical regions whose main input is not from the thalamus, but from other cortical regions.

We tested the connectivity hypothesis for the case of the VWFA^{10–14}, a ventrolateral region that responds much more strongly to visually presented words or letter strings than to other visually similar stimuli, including digit strings, faces and words written in an unfamiliar orthography (for example, Chinese or Hebrew for English speakers)¹⁵. Notably, these patterns develop with reading experience and ability

and are only present in readers¹¹. According to the connectivity hypothesis, the eventual cortical site of the VWFA should be predicted by its earlier-developing extrinsic connections to other brain regions, that is, pre-reading connectivity patterns should predict the eventual location of the VWFA after a child learns to read. Alternative (but not mutually exclusive) hypotheses are that the location of the VWFA is determined by the intrinsic molecular or circuit properties of that piece of cortex or by pre-existing featural^{16–19} or retinotopic selectivities that predispose this region to develop orthographic selectivity. To test the connectivity hypothesis, we scanned children longitudinally both before and after they learned to read, and tested whether the VWFA develops in this interval, and whether the specific location at which the VWFA develops is predictable from the connectivity fingerprint of that same region before children learn to read.

RESULTS

Functional selectivity of VWFA and IFFA

We defined a word-selective VWFA in each individual's age 8 data as any voxels that responded more strongly to words than line drawings of objects (at $P < 0.005$ uncorrected in half the functional runs) in a VWFA constraint region (**Supplementary Fig. 1** and Online Methods). We defined face-selective cortex similarly (that is, any voxels in a left fusiform face area (IFFA) constraint region that responded more strongly to line drawings of faces than to line drawings of objects, at $P < 0.005$ in half the functional runs).

We found both a VWFA and IFFA in 29 of 31 (94%) of the children that we scanned at age 8. Given that 14 of these children could not yet read at age 5 and had a functional magnetic resonance imaging (fMRI) scan at age 5, our main fMRI analyses focused on this cohort.

¹Department of Brain and Cognitive Sciences, Massachusetts Institute of Technology, Cambridge, Massachusetts, USA. ²McGovern Institute for Brain Research, Massachusetts Institute of Technology, Cambridge, Massachusetts, USA. ³Department of Psychological and Brain Sciences, Boston University, Boston, Massachusetts, USA. ⁴Department of Communication Sciences and Disorders, Northwestern University, Evanston, Illinois, USA. ⁵Department of Biological Sciences, Barnard College, Columbia University, New York, New York, USA. ⁶Boston Children's Hospital, Boston, Massachusetts, USA. Correspondence should be addressed to Z.M.S. (zsaygin@mit.edu).

Received 5 January; accepted 5 July; published online 8 August 2016; doi:10.1038/nn.4354

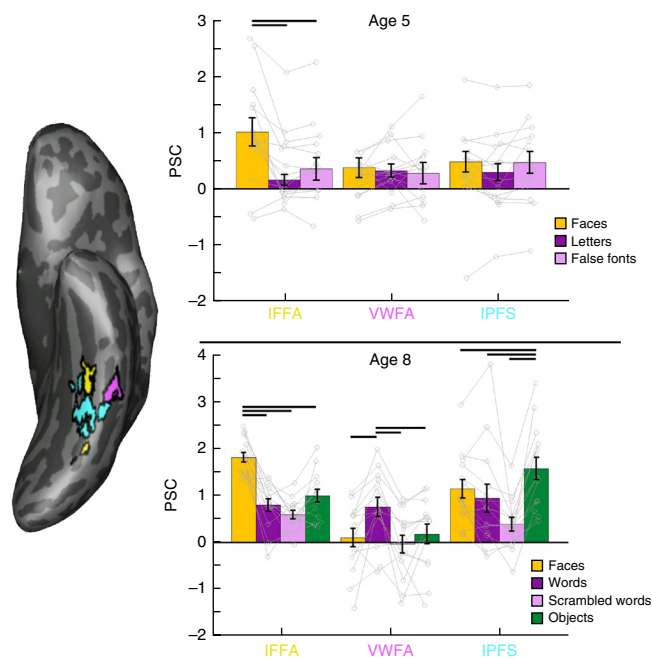
Figure 1 Percent signal change (PSC) for each fROI. Left, inflated surface of an example subject showing each of their fROIs defined from age 8 data (IFFA in yellow, VWFA in magenta, IPFS in cyan). Top, mean PSCs at age 5 in fROIs defined on age 8 data (registered to 5-year-old brain). Before a child was able to read, there was no selectivity to letters, letter-like stimuli (false fonts) or faces in the region that later became the VWFA, whereas IFFA showed clear selectivity for faces even at this age. Bottom, mean PSCs at age 8. We found clear selectivity for faces in IFFA and clear selectivity for words in the VWFA at age 8 in data not used to define the fROI. Error bars denote s.e.m. Horizontal bars reflect significant *post hoc* paired *t* tests ($N = 14$; *P* values: age 8, IFFA: faces vs. words 1.25×10^{-5} , faces vs. scrambled words 1.15×10^{-7} , faces vs. objects 3.05×10^{-7} ; VWFA: words vs. scrambled words 4.57×10^{-4} , words vs. objects 1.68×10^{-3} , words vs. faces 2.68×10^{-3} , IPFS: objects vs. words 9.71×10^{-4} , objects vs. scrambled words 4.20×10^{-6} , objects vs. faces 1.76×10^{-2} ; age 5, IFFA: faces vs. letters 1.18×10^{-3} , faces vs. false fonts 2.44×10^{-3}).

At age 8, all of these children could read and had both a VWFA and IFFA (Online Methods). We extracted the magnitude of response (percent signal change from a no-stimulus baseline) from these regions for each of the stimulus categories in fMRI runs independent of those used to define the regions at age 8 (Fig. 1). The VWFA and IFFA were clearly distinct in their responses to the stimulus categories (two-way repeated-measures ANOVA of functional region of interest (fROI) \times condition: $F_{3,78} = 24.56$, $P = 2.72 \times 10^{-11}$). The VWFA responded more strongly to words than it did to other visually similar stimuli, including line drawings of faces, scrambled words and line drawings of objects (repeated-measures ANOVA by condition: $F_{3,39} = 10.96$, $P = 2.34 \times 10^{-5}$; Fig. 1). The IFFA responded more strongly to line drawings of faces than to objects, words and scrambled words ($F_{3,39} = 34.30$, $P = 5.03 \times 10^{-11}$; Fig. 1).

No evidence for early functional differentiation of VWFA

We then measured the response profiles of these same fROIs at age 5, before these children learned to read, by registering each child's age 8 VWFA and IFFA to their own fMRI data at age 5 (Online Methods). We found that VWFA was not selective to orthography at pre-reading: the VWFA did not show any selectivity to letters over faces or false font letters (repeated-measures ANOVA by condition: $F_{2,26} = 1.67$, $P = 0.21$; Fig. 1), whereas the IFFA already showed strong selectivity to faces over letters or false fonts even at age 5 ($F_{2,26} = 14.02$, $P = 7.41 \times 10^{-5}$; Fig. 1). Additional analyses (Online Methods) revealed that the VWFA in adults responds similarly to words and individual letters; thus, the use of individual letters in the 5-year-old children should be a good measure of the selectivity of this region.

Furthermore, to test whether our fMRI methods at age 5 (stimuli and scanning parameters) were sufficient to detect a VWFA at age 5 if it were present, we also analyzed a small group of children ($n = 8$) who could read at age 5 and who were scanned again at age 8 (readers). We performed three different types of analyses in these children and compared them to the pre-readers. First, we found that the VWFA (defined at age 8) did show significant selectivity to letters at age 5 in children who could already read at that age. This analysis revealed that we can detect word and letter selectivity when it is present at age 5, with the same contrasts and scanning parameters used in the main cohort of children who could not read at age 5 (Supplementary Fig. 2). Second, to test the hypothesis that letter selectivity may have been present at age 5, but in a different location from the same child's VWFA at age 8, we performed a 'binned analysis' that did not rely on localization in the age 8 data. We again found that children who could not read at age 5 did not show selectivity to letters versus false fonts or faces (Fig. 2), but children who could read at age 5 showed selectivity to



both letters versus false fonts and letters versus faces (Supplementary Fig. 3). Both groups showed selectivity for words at age 8 (when they could all read). This analysis further bolsters the conclusion that there is no word and letter selectivity at age 5 in children who cannot read. Third, using a multi-voxel pattern analysis (that is, correlation of voxel-wise signal between and across stimulus conditions²⁰), we found that classification accuracy was at chance for discriminating letters (from faces or false fonts) in the age 5 data from children who could not read at age 5 when tested in that child's 8-year-old VWFA fROI. In contrast, classification performance was significantly above chance for letters (versus false fonts or faces) in children who could already read at age 5 (Supplementary Fig. 4). Note that the VWFA in the early readers was defined using only age 8 data; the age 5 data only had three stimulus conditions and therefore could not be used to define the contrast of words > objects (which we refer to in the rest of the study, and has been used to define the VWFA previously; for example, see ref. 15). However, the three conditions at age 5 were sufficient to show a letter-preferring region only in the readers at that age. Altogether, our results show that the region that will later become the VWFA cannot discriminate letters from non-letter stimuli before children can read. The characteristic functional selectivity of the VWFA is found only in children who can read.

These data also show that, although the VWFA is not selective for orthography in children who cannot read, the IFFA is already selective for faces at age 5. Note that we also found no selectivity for faces in the VWFA at age 5 in these children (as reported above) and that there was no change in the VWFA's response to faces from age 5 to age 8 ($P = 0.927$; $T(13) = 0.094$). These data suggest that early feature selectivity in the VWFA (at least for the stimuli that we tested) does not determine its later functional profile. Other evidence against this hypothesis comes from an analysis of left posterior fusiform sulcus (IPFS), a nearby region that responds selectively to shape¹⁷ (Fig. 1). The response profile of the VWFA and adjacent IPFS (defined at age 8 and registered to the 5-year-old data) were not significantly different from each other at age 5 (fROI \times condition repeated measure ANOVA: $F_{2,52} = 1.64$, $P = 0.20$), but were at age 8 (for the same subjects and same three conditions as age 5, that is, no objects condition; fROI \times condition ANOVA: $F_{2,52} = 5.59$, $P = 7.06 \times 10^{-8}$). These

Figure 2 PSC in the VWFA as a function of fROI volume. To further test whether there was any selectivity for orthography at age 5, we performed a 'binned' analysis in which we used one run of age 5 data to define the N th percentile of letter-selective voxels anywhere in the larger VWFA parcel (that is, constraint region in **Supplementary Fig. 1** based on independent data in adults); we then measured the PSC to each condition in the other run of age 5 fMRI data in those same voxels. Children who were not able to read at age 5 did not show selectivity for letters as compared to faces or false fonts (top). The analogous analysis of the age 8 data in the same children (bottom) found strong selectivity for words. Error bars reflect s.e.m. for $N = 14$ subjects.

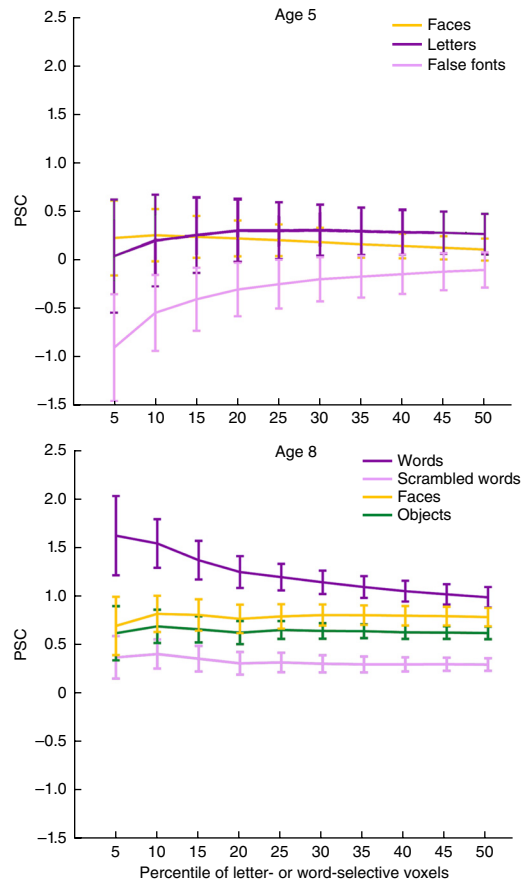
data provide no evidence that the cortical tissue that will become the VWFA is earmarked for that function by a distinctive functional response before word selectivity develops. They also argue against the hypotheses that the VWFA takes over cortical regions that were previously selective for object shape or faces^{16,18,19,21}.

Testing the connectivity hypothesis for word selectivity

We next tested the hypothesis that pre-existing connectivity determines the location of the VWFA by asking whether each child's voxel-by-voxel connectivity data at age 5 can predict the location of the same child's word selectivity at age 8. 11 children had a useable diffusion-weighted scan (DWI) at age 5, so our longitudinal DWI analyses focused on this cohort (the fMRI selectivity results remained the same as above even in these 11 children; **Supplementary Table 1**). We focused on the left occipitotemporal anatomical parcel (that is, combined Freesurfer parcel of fusiform and inferior temporal cortex; IOTC parcel) and trained a model to learn the relationship between the connectivity of each voxel in this region at age 5 and fMRI activation patterns at age 8 in the same individuals, and tested the model on new children (in a leave-one-out manner; Online Methods), as described previously^{1,2} and adapted in other studies²². We found that early connectivity was able to predict the later spatial profile of word selectivity in these children (**Fig. 3**); the correlation across voxels in the left occipitotemporal parcel between the actual fMRI t statistic values for words > objects at age 8 and the predicted fMRI values from connectivity was 0.47 ± 0.036 (mean Fisher z across all subjects). These predictions were significantly better than chance for each subject individually at $P < 0.05$ (based on random permutations exact tests per subject; $P = 0.014$ for one subject, $P = 0$ for all other subjects).

To better assess the strength of these DWI predictions and how well they captured individual differences in spatial patterns of functional selectivity, we compared the DWI predictions to predictions generated from the fMRI data of other subjects at age 8. First, we generated group average predictions: we performed a random effects analysis on the words > objects contrast data from all but one subject in template space and mapped these values to the native space data of the subject we left out. This procedure generated voxel-wise neural responses for word selectivity in each individual based on aggregate responses from all other participants. We found that the correlations between actual and predicted word selectivity from this group average analysis were much lower (mean Fisher $z = 0.26 \pm 0.042$; **Fig. 4**) than the predictions from the same individual's connectivity (paired t test of Fisher z correlations of DWI predictions versus group-average predictions: $T_{10} = 5.63$; $P = 2.20 \times 10^{-4}$).

Next, we compared the DWI predictions to predictions generated from each other subject's fMRI data individually. We registered each child's fMRI data from age 8 to each other child's DWI data at age 5, and generated voxel-wise predictions for each subject on the basis of every other child's data. These predictions were less accurate than the



predictions of an individual's own fMRI data (mean Fisher z : 0.25 ± 0.027 ; $T_{10} = 6.85$; $P = 4.48 \times 10^{-5}$; **Fig. 4**). Thus, each individual's connectivity data at age 5 better predicted the same child's functional activation pattern at age 8 than did another child's fMRI data. These results indicate that the prediction of functional activation patterns from connectivity at age 5 is spatially precise enough to predict individual differences in functional activation patterns.

Random permutations represent the lowest bar that the DWI predictions should surpass to be considered accurate. To get an idea of the best possible predictive correlation values, we asked how well half of each individual's own fMRI data at age 8 would predict the other half of fMRI data in the same subject (that is, split-half reliability of age 8 fMRI data). The predictions reported above were generated from all of the fMRI data; for direct comparability with the same amount of data in each case, we next generated predictions from DWI connectivity from half the fMRI data ($z = 0.46 \pm 0.041$) and compared these predictions to predictions from the split-half fMRI data ($z = 0.69 \pm 0.086$; **Fig. 3c**). As expected, the split-half correlations outperformed predictions from age 5 DWI ($T_{10} = 3.87$, $P = 3.09 \times 10^{-3}$). Children with higher correlation values between actual versus predicted also had higher scan-to-scan reliability ($R = 0.77$, $P = 5.63 \times 10^{-3}$). After normalizing for scan-to-scan reliability (which included the same amount of fMRI data as the DWI predictions), we found that connectivity predicted about 70% of the reliable variance in words > objects responses ($R^2 = 0.69 \pm 0.015$).

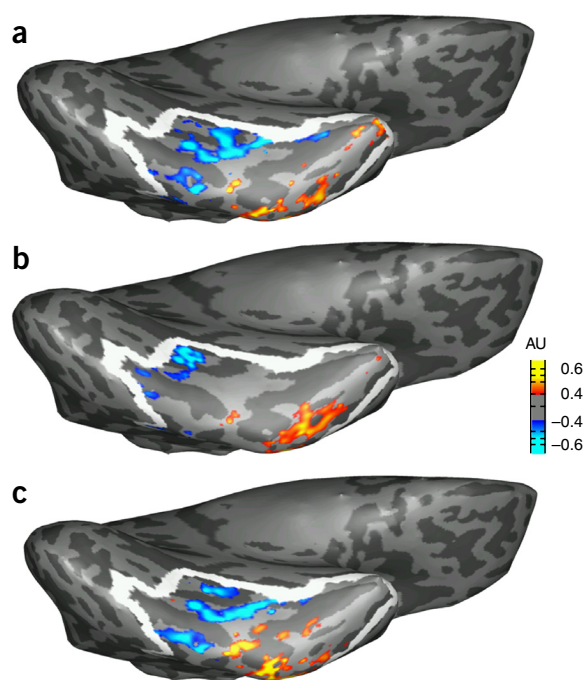
We also compared the longitudinal DWI predictions of word selectivity to predictions of face selectivity, which were generated in exactly the same manner (age 5 DWI to predict age 8 fMRI). Predictions of word selectivity were comparable to predictions of face selectivity ($z = 0.47 \pm 0.036$ versus 0.43 ± 0.061 respectively; t test of correlation

Figure 3 Actual versus predicted fMRI activation for words > objects on the ventral surface of an example subject. Heat map reflects word selectivity and white outline indicates the boundaries of the left occipitotemporal anatomical parcel. AU = arbitrary units. (a) Actual fMRI activation for words > objects at age 8. (b) Activation that is predicted from the same individual's DWI data at age 5. (c) Activation that is predicted from the same individual's fMRI data at age 8, from independent, left-out fMRI runs from a. This split-half reliability illustrates the best possible predictions that one could make about an individual's word selectivity. The predicted activation from DWI matches the actual activation pattern, capturing loci that are accurately predicted from left-out data. Note that all images (actual, predicted from DWI and predicted from left-out data) are based on (or trained on) an equal number of fMRI runs.

values for word- versus face-selectivity predictions: $T_{10} = 0.50$, $P = 0.63$). Using DWI data collected at age 8, we also compared the longitudinal predictions to the within time-point predictions. We generated predictions of age 8 word selectivity from age 8 DWI data and found no significant difference between the across-time predictions versus within-time predictions ($T_{10} = 1.42$, $P = 0.19$).

We then asked how well connectivity predicted the VWFA fROI in particular, that is, not the full gradient of words > objects responses in the large anatomical occipitotemporal parcel, but the thresholded and positive (that is, word selective) responses in the VWFA constraint region (that is, the smaller region that contains the VWFA fROI in most subjects, or GSS parcel; Online Methods). For each subject, we created a VWFA fROI from the DWI-predicted activations and compared it to the same subject's actual functionally defined VWFA. We found that the predicted VWFA overlapped with the actual VWFA by 64% (overlap coefficient = 0.635 ± 0.058 ; ranging from 0.84 ± 0.03 for the most lenient thresholds to 0.45 ± 0.09 for highest thresholds; the overlap coefficient is defined as the size of intersection divided by the smaller of the two sets and equals 1 if an fROI is a subset of the other). We also looked at how far away the predicted VWFA was from the actual VWFA. We used the modified Hausdorff metric, which describes the mean distance of all points in the predicted fROI from the closest points in the actual fROI. The VWFA predicted from DWI was on average 0.65 ± 0.12 voxels (1.3 ± 0.4 mm) away from the actual VWFA (ranging from 0.49 ± 0.11 voxels or 0.98 ± 0.22 mm for the most lenient thresholds to 0.98 ± 0.28 or 1.96 ± 0.56 mm for highest thresholds). That is, the estimated VWFA location from the DWI-predicted data was less than one voxel, or 1.3 mm on average, away from an individual's true VWFA. As a comparison, the VWFA fROI generated from the split-half fMRI data (that is, best possible overlap metric) had an overlap coefficient of 0.865 ± 0.014 and Hausdorff metric of 0.26 ± 0.049 voxels.

These results strongly suggest that the VWFA already has distinct connectivity patterns, even at age 5, when a child cannot yet read and when that same cortical region shows no orthographic selectivity. Our final analyses asked what these distinct connectivity patterns



were; specifically, we defined the VWFA and two adjacent fROIs (IFFA and IPFS) and compared the connectivity patterns of each of these fROIs to the rest of the brain. We ran tractography on the age 5 data from each fROI (VWFA, IFFA and IPFS, defined on the age 8 data and registered to the age 5 data) to every other brain region (defined anatomically from Freesurfer sulcal/gyral segmentation). We first performed an ANOVA of seed (VWFA, IFFA, or IPFS) \times target. We found a significant main effect of seed ($F_{2,2430} = 18.54$, $P = 1.02 \times 10^{-8}$) and significant seed \times target interaction ($F_{160,2430} = 3.39$, $P = 2.20 \times 10^{-37}$), indicating significant differences in the connectivity patterns for different fROIs. To further explore the differences between VWFA and either the IFFA or IPFS, we subsequently ran a two-way ANOVA of VWFA versus IFFA \times target and VWFA versus IPFS \times target separately. The VWFA was significantly more connected in general than the IFFA (significant main effect; $F_{1,1620} = 30.01$, $P = 4.97 \times 10^{-8}$); these were not global differences in connectivity, but were rather a result of differences between the two fROIs in their connectivity to certain target regions (interaction effect, $F_{80,1620} = 1.92$, $P = 3.64 \times 10^{-6}$). Specifically, the VWFA was more strongly connected than IFFA was to left-lateralized temporal and frontal parcels (middle temporal: $P = 3.41 \times 10^{-4}$, $T(10) = 5.31$; superior temporal: $P = 1.44 \times 10^{-2}$, $T(10) = 2.95$; transverse temporal: $P = 4.29 \times 10^{-2}$, $T(10) = 2.32$; lateral orbitofrontal: $P = 4.30 \times 10^{-2}$, $T(10) = 2.32$), which may correspond with putative language regions (consistent with recent tractography studies in adults^{23,24}), as well as the left precentral gyrus ($P = 4.28 \times 10^{-2}$, $T(10) = 2.32$), inferior parietal ($P = 2.93 \times 10^{-2}$, $T(10) = 2.54$), entorhinal cortex ($P = 3.18 \times 10^{-2}$, $T(10) = 2.49$), ventral diencephalon

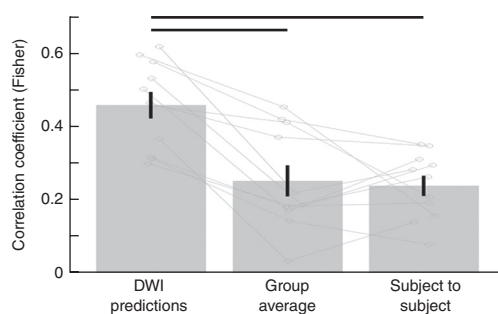


Figure 4 Correlations of actual word selectivity at age 8 with predicted word selectivity. Predictions of age 8 word selectivity from age 5 DWI data were compared to predictions from the age 8 fMRI data of all other subjects (group average) and to predictions from each other subject's age 8 data. DWI predictions outperformed both of these types of predictions, demonstrating that the prediction of functional activation patterns from connectivity at age 5 is spatially precise enough to predict individual differences in functional activation patterns. Horizontal bars reflect significant differences (paired t tests, each $P < 0.05 \times 10^{-4}$, $N = 11$); error bars reflect s.e.m.

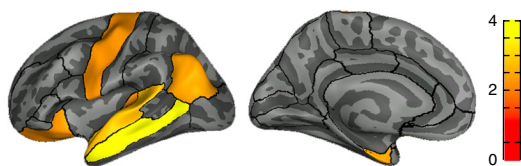


Figure 5 Left-lateralized regions that are preferentially connected with the VWFA versus IFFA or IPFS at age 5. Color bar reflects t values from the VWFA versus IFFA comparison (*post hoc* paired t tests, $P < 0.05$). Connectivity (of the region that will become the VWFA) to these regions was already elevated (compared to nearby cortex) at age 5, even when no evidence of functional differentiation existed in the VWFA at that age.

($P = 4.49 \times 10^{-2}$, $T(10) = 2.29$) and putamen ($P = 4.56 \times 10^{-2}$, $T(10) = 2.28$; cortical targets displayed in **Fig. 5**). We also found differences between the VWFA and IPFS in their connectivity to specific target regions (main effect not significant: $F_{1,1620} = 1.70$, $P = 0.19$; interaction effect significant: $F_{80,1620} = 2.82$, $P = 1.67 \times 10^{-14}$). The VWFA was more connected than IPFS with the left middle temporal gyrus ($P = 2.90 \times 10^{-3}$, $T(10) = 3.91$), whereas the IPFS was more connected than the VWFA with only the left lingual gyrus ($P = 3.76 \times 10^{-4}$, $T(10) = -5.25$; **Fig. 5**). The VWFA's connectivity with the rest of the brain at age 5 is therefore distinct from the connectivity patterns of both the adjacent IPFS and IFFA, despite a lack of functional differentiation at this age.

In conclusion, these results indicate that the precise location of the VWFA is accurately predicted from the connectivity of this region even before the functional specialization for orthography in VWFA exists. fMRI selectivity to words does not exist before a child learns to read, but there are already differences in the connectivity fingerprints of voxels that will later become word selective.

DISCUSSION

The human cerebral cortex contains dozens of functionally distinct regions, each arising in approximately the same location in almost every normal adult. How does this intricate and systematic organization arise in development? We tested the hypothesis that the functional fate of a given cortical region may be determined by its earlier-developing pattern of connections with the rest of the brain, that is, its connectivity fingerprint. Consistent with this hypothesis, we found that the functional selectivity of VWFA arose between age 5 and age 8, when children learned to read, and that its cortical location at age 8 could be predicted by the distinctive connectivity of the same region at age 5, before the child could read and before the region differed functionally from nearby more general shape-responsive cortex.

The ability to predict the spatial pattern of word selectivity across the ventral pathway from earlier-developing voxel-wise patterns of connectivity was robust, accounting for 69% of the reliable variance in word selectivity across voxels. Furthermore, these predictions accounted for individual differences in the precise location of the VWFA, as the location of each 8-year-old child's VWFA was better predicted by that child's own connectivity data at age 5 than it was by another child's connectivity pattern at age 5, or even by a group analysis of word selectivity in all of the other children at age 8. Finally, we found no evidence that functional response profiles at age 5 could predict word selectivity at age 8. In particular, our finding that the region that becomes the VWFA did not respond differentially to faces versus letters before children learned to read argues against prior hypotheses that the region that becomes the VWFA starts out with a selectivity for letter-like features^{16–18} or faces¹⁹. Taken together,

these findings powerfully support the idea that earlier-developing patterns of connectivity instruct the development of cortical regions into functionally distinct regions.

Our results provide evidence for an instructive role of connectivity in cortical development that dovetails with the classic studies of 'rewired' ferrets. In those studies, the cortical region that would otherwise have developed into primary auditory cortex instead took on many of the distinctive functional signatures of primary visual cortex after retinal input was rerouted (via MGN) to that location^{5–9}. Our findings extend the principle from primary sensory regions in ferrets to high-level cortical regions in humans.

Myriad questions remain for future research. First, although we found no evidence for a distinctive functional response at age 5 in the region that would later become the VWFA, this finding should be more extensively tested with a broader range of stimuli. One prior study²⁵ reported symbol selectivity in a nearby location in four-year-old children, but because that study used a cross sectional design it is possible that the region showing symbol selectivity at age 4 is different from the region that became the VWFA. Of particular interest is whether this region shows selectivity for foveal versus peripheral inputs, rectilinear versus curvilinear features, or any other feature bias that may predispose this region to become selective for visually presented words and letters.

A second important question is whether early connectivity also instructs functional development of other functionally distinctive extrastriate regions. This question will be difficult to answer given the great challenges of scanning children younger than 5 years of age, when face-selective regions are already evident in our data (but see ref. 25, which found no evidence of face selectivity in the left fusiform in 4-year-old children). Pending such studies, it remains possible that the developmental mechanisms that give rise to the VWFA may differ from those for other cortical regions whose selectivity may be less dependent on experience.

Third, although the strong cross-lagged correlations we found in individuals are suggestive of a causal role of connectivity in determining later function, a direct causal test has yet to be run. Such a test may be possible in the future by testing humans who sustained early disruptions of the relevant white matter connections, for example, from stroke. Our results accord with previous correlational studies showing that white matter bundles predict future reading ability in children who cannot yet read (and may indicate a structural basis of behavioral risk for dyslexia that predates reading instruction^{26,27}). Future studies can investigate how pre-reading connectivity constrains future reading ability in individual subjects, and what aspects of this connectivity are malleable by early experience.

Finally, showing that distinctive connectivity arises before distinctive function begs the question of how the connectivity fingerprint itself arose. Possible mechanisms that may determine patterns of connectivity, or that may work in tandem with connectivity to determine function, include molecular markers or tissue and circuit properties inherent in each cortical region (for example, cytoarchitecture^{28,29}). A combination of work on animal models, as well as longitudinal studies and experiments of nature in humans, should be able to resolve these questions, providing a rich new picture of the mechanisms underlying the development of the human cortex.

In sum, our longitudinal, cross-lagged study supports the hypothesis that early connectivity instructs the functional development of the VWFA, a cortical region that underlies the uniquely human ability to read. Furthermore, the ability to predict later brain function from an anatomical scan that can be performed even in a sleeping infant

may offer powerful new strategies for understanding and diagnosing neurodevelopmental disorders such as dyslexia and autism.

METHODS

Methods and any associated references are available in the [online version of the paper](#).

Note: Any Supplementary Information and Source Data files are available in the online version of the paper.

ACKNOWLEDGMENTS

We thank B. Fischl and M. Reuter for their guidance and advice on longitudinal registration, S. Robinson and O. Ozernov-Palchik for assistance with participant coordination and A. Park for technical assistance. We thank the Athinoula A. Martinos Imaging Center at the McGovern Institute for Brain Research at the Massachusetts Institute of Technology and its staff. We also thank our READ Study research testers, school coordinators and principals, and participating families. This work was funded by NICHD/NIH grant F32HD079169 to Z.M.S., NIH/NICHD R01HD067312 to J.D.E.G. and N.G., Ellison Medical Foundation, EY13455 to N.K., and grant 1444913 from McGovern Institute for Brain Research MINT to N.K. and Z.M.S.

AUTHOR CONTRIBUTIONS

Z.M.S., D.E.O. and N.K. designed the experiments. Z.M.S., E.S.N., D.A.Y., S.D.B., N.G., J.D.E.G. and N.K. conducted the experiments or supplied data. Z.M.S., D.E.O., D.A.Y. and J.F. analyzed the data. Z.M.S., D.E.O. and N.K. wrote the manuscript.

COMPETING FINANCIAL INTERESTS

The authors declare no competing financial interests.

Reprints and permissions information is available online at <http://www.nature.com/reprints/index.html>.

- Saygin, Z.M. *et al.* Anatomical connectivity patterns predict face selectivity in the fusiform gyrus. *Nat. Neurosci.* **15**, 321–327 (2012).
- Osher, D.E. *et al.* Structural connectivity fingerprints predict cortical selectivity for multiple visual categories across cortex. *Cereb. Cortex* **26**, 1668–1683 (2015).
- Mahon, B.Z. & Caramazza, A. What drives the organization of object knowledge in the brain? *Trends Cogn. Sci.* **15**, 97–103 (2011).
- Hannagan, T., Amedi, A., Cohen, L., Dehaene-Lambertz, G. & Dehaene, S. Origins of the specialization for letters and numbers in ventral occipitotemporal cortex. *Trends Cogn. Sci.* **19**, 374–382 (2015).
- Sur, M., Garraghty, P.E. & Roe, A.W. Experimentally induced visual projections into auditory thalamus and cortex. *Science* **242**, 1437–1441 (1988).
- Roe, A.W., Pallas, S.L., Hahn, J.O. & Sur, M. A map of visual space induced in primary auditory cortex. *Science* **250**, 818–820 (1990).
- Roe, A.W., Pallas, S.L., Kwon, Y.H. & Sur, M. Visual projections routed to the auditory pathway in ferrets: receptive fields of visual neurons in primary auditory cortex. *J. Neurosci.* **12**, 3651–3664 (1992).
- Sharma, J., Angelucci, A. & Sur, M. Induction of visual orientation modules in auditory cortex. *Nature* **404**, 841–847 (2000).
- Hornig, S. *et al.* Differential gene expression in the developing lateral geniculate nucleus and medial geniculate nucleus reveals novel roles for *Zic4* and *Foxp2* in visual and auditory pathway development. *J. Neurosci.* **29**, 13672–13683 (2009).
- McCandliss, B.D., Cohen, L. & Dehaene, S. The visual word form area: expertise for reading in the fusiform gyrus. *Trends Cogn. Sci.* **7**, 293–299 (2003).
- Dehaene, S. *et al.* How learning to read changes the cortical networks for vision and language. *Science* **330**, 1359–1364 (2010).
- Glezer, L.S., Jiang, X. & Riesenhuber, M. Evidence for highly selective neuronal tuning to whole words in the “visual word form area”. *Neuron* **62**, 199–204 (2009).
- Glezer, L.S. & Riesenhuber, M. Individual variability in location impacts orthographic selectivity in the “visual word form area”. *J. Neurosci.* **33**, 11221–11226 (2013).
- Glezer, L.S., Kim, J., Rule, J., Jiang, X. & Riesenhuber, M. Adding words to the brain's visual dictionary: novel word learning selectively sharpens orthographic representations in the VWFA. *J. Neurosci.* **35**, 4965–4972 (2015).
- Baker, C.I. *et al.* Visual word processing and experiential origins of functional selectivity in human extrastriate cortex. *Proc. Natl. Acad. Sci. USA* **104**, 9087–9092 (2007).
- Srihasam, K., Vincent, J.L. & Livingstone, M.S. Novel domain formation reveals proto-architecture in inferotemporal cortex. *Nat. Neurosci.* **17**, 1776–1783 (2014).
- Grill-Spector, K., Kourtzi, Z. & Kanwisher, N. The lateral occipital complex and its role in object recognition. *Vision Res.* **41**, 1409–1422 (2001).
- Dehaene, S. & Cohen, L. Cultural recycling of cortical maps. *Neuron* **56**, 384–398 (2007).
- Dehaene, S. & Cohen, L. The unique role of the visual word form area in reading. *Trends Cogn. Sci.* **15**, 254–262 (2011).
- Haxby, J.V. *et al.* Distributed and overlapping representations of faces and objects in ventral temporal cortex. *Science* **293**, 2425–2430 (2001).
- Behrmann, M. & Plaut, D.C. Distributed circuits, not circumscribed centers, mediate visual recognition. *Trends Cogn. Sci.* **17**, 210–219 (2013).
- Tavor, I. *et al.* Task-free MRI predicts individual differences in brain activity during task performance. *Science* **352**, 216–220 (2016).
- Bouhali, F. *et al.* Anatomical connections of the visual word form area. *J. Neurosci.* **34**, 15402–15414 (2014).
- Yeatman, J.D., Rauschecker, A.M. & Wandell, B.A. Anatomy of the visual word form area: adjacent cortical circuits and long-range white matter connections. *Brain Lang.* **125**, 146–155 (2013).
- Cantlon, J.F., Pinel, P., Dehaene, S. & Pelphrey, K.A. Cortical representations of symbols, objects, and faces are pruned back during early childhood. *Cereb. Cortex* **21**, 191–199 (2011).
- Saygin, Z.M. *et al.* Tracking the roots of reading ability: white matter volume and integrity correlate with phonological awareness in prereading and early-reading kindergarten children. *J. Neurosci.* **33**, 13251–13258 (2013).
- Langer, N. *et al.* White matter alterations in infants at risk for developmental dyslexia. *Cereb. Cortex* <http://dx.doi.org/10.1093/cercor/bhv281> (2015).
- Brodman, K. *Vergleichende Lokalisationslehre der Grosshirnrinde in ihren Prinzipien dargestellt auf Grund des Zellenbaues* (Barth, 1909).
- Lorenz, S. *et al.* Two new cytoarchitectonic areas on the human mid-fusiform gyrus. *Cereb. Cortex* <http://dx.doi.org/10.1093/cercor/bhv225> (2015).

ONLINE METHODS

Participants. As part of a larger study, children completed a short battery of psychoeducational assessments in their schools in New England in the spring of pre-kindergarten or fall of kindergarten, before formal word reading instruction. A subset of children who completed screening were invited to participate in the brain imaging study. This study was approved by the institutional review boards at the Massachusetts Institute of Technology and Boston Children's Hospital. Parents gave written consent and children gave verbal assent to participate.

We collected DWI data and/or fMRI data from 112 children in pre-k or kindergarten (age 5 group). Three years later, we invited all children back to participate in another MRI study (which included both DWI and fMRI) after they completed second grade (age 8 group). 33 children agreed to return and were scanned after completing second grade; two individuals were excluded either for poor scan quality or for withdrawing from the study at the time of the scan. 20 of these children (pre-readers) were unable to read more than five high-frequency short words (WRMT-R/NU Word ID subtest³⁰) when tested at age 5. We focused our analyses on these children because they could not read at the time of their pre-kindergarten scan.

9 of 20 children were excluded from longitudinal predictions analysis (six did not have a kindergarten DWI scan; three had excessive DWI motion as determined by visual inspection; see **Supplementary Table 3** for DWI and fMRI motion measures). Thus, the longitudinal fMRI analysis included 14 children (4 females and 11 males, 5.4 ± 0.09 years old at first scan, and 8.3 ± 0.07 years old at second scan) and the longitudinal DWI prediction analysis included 11 children (5 females and 6 males, 5.5 ± 0.08 years at first scan, and 8.4 ± 0.05 years at second scan). All children met eligibility criteria including: being a native speaker of American English; born after at least 36 weeks gestation; no sensory or perceptual difficulties other than corrected vision; no history of head or brain injury or trauma; no neurological, neuropsychological, or developmental diagnoses; no medications affecting the nervous system; standard scores > 80 on measures of nonverbal IQ and vocabulary at age 5 (Kaufman Brief Intelligence Test [KBIT-2] Matrices³¹; Peabody Picture Vocabulary Test [PPVT-4]³²).

Structural image acquisition and processing. Structural, DWI, and fMRI data for both time points were acquired on a 3T Siemens Trio Tim MRI scanner with a standard Siemens 32-channel phased array head coil. A whole-head, high-resolution T1-weighted multiecho MPRAGE³³ anatomical volume was acquired at each time point (acquisition parameters: TR = 2,350 ms, TE = 1.64 ms, TI = 1,400 ms, flip angle = 7°, FOV = 192 × 192, 176 slices, voxel resolution = 1.0 mm³, acceleration = 4). An online prospective motion correction algorithm reduced the effect of motion artifacts during the structural scan, and 10 selective reacquisition images were acquired and included to replace images that were affected by head motion³⁴.

Structural MRI data were processed using a semiautomated processing stream using the default parameters in FreeSurfer v5.2.0 (<http://surfer.nmr.mgh.harvard.edu/>)^{35–38}, which includes motion and intensity correction, surface coregistration, spatial smoothing, subcortical segmentation, and cortical parcellation based on spherical template registration. The resulting cortical parcellation and subcortical segmentations were individually edited and reviewed for quality control and were used as seeds and targets for DWI tractography (below).

fMRI protocols. Age 5. Children viewed two runs of 20-s blocks of black and white photographs of neutral expression faces, white letters, white false font stimuli, and a fixation condition (a total of six blocks per stimulus type). Stimuli were 800 × 800 pixels and presented on a black background. False font stimuli were generated by rearranging parts of the same real letters and following orthographic patterns of English letters (for example, no letter had ascending and descending aspects; **Supplementary Fig. 2**). Stimuli were presented for 1,500 ms followed by a fixation cross for 500 ms, for a total duration of 2,000 ms. Each run lasted 4 min and 8 s and consisted of three blocks each of letters, faces, false font letters and fixation. Participants performed a one-back task, responding with a button-press to any image presented twice in a row (see **Supplementary Table 2** for accuracies).

Age 8. Children viewed 6 runs of 18-s blocks (26 stimuli + 2 repetitions per block) of black and white line-drawings of faces, objects, words, scrambled words and a fixation condition (**Supplementary Fig. 1**). Line drawings were 300 × 300 pixels, and words were of height 120 pixels with width determined by the length

of the word (minimum 120 pixels and maximum 300 pixels). A gray square grid with spacing 30 × 30 pixels was placed over all images to best equate the different stimulus categories to the scrambled stimuli. To create the scrambled stimuli, the square sections of the gridded image were randomized. All stimuli were overlaid on a single-color background that changed color every 500 ms. Stimuli were presented for 500 ms with an ISI of 192.3 ms (692 ms per trial). Each run consisted of 19 blocks (four blocks per category and three fixation blocks per run) and participants performed a one-back task, responding with a button-press for any image presented twice in a row.

fMRI acquisition parameters. Age 5. Data were collected with 3 × 3 × 4-mm resolution, 2-s TR, 30-ms TE, 90° flip, 172 TRs, 64 × 64 base resolution, 32 slices approximately parallel to AC/PC line to cover the entire cortex. Prior to each scan, four images were acquired and discarded to allow longitudinal magnetization to reach equilibrium. PACE, an online prospective motion correction algorithm³⁹, was implemented to reduce the effect of motion artifacts.

Age 8. Data were collected with 2-mm³ resolution, 2-s TR, 30-ms TE, 90° flip, 172 TRs, 100 × 100 base resolution, 25 slices approximately parallel to the base of the temporal lobe to cover the entire inferior temporal cortex. We also collected a field map for distortion correction every two runs with the same slice prescription as the fMRI sequence (25 slices, 2-mm³ resolution, 500-ms TR, 55° flip, 100 × 100 base resolution).

fMRI analysis. Age 5 fMRI data were analyzed using Nipype (<http://nipype.org/nipype/index.html>)⁴⁰. Images were motion corrected using MCFLIRT and high-pass temporal filtering (using a cutoff of 120s). Functional images were coregistered to anatomical space using bbgregister. Statistical analyses were conducted in FSL. Age 8 fMRI data were analyzed with Freesurfer (<http://surfer.nmr.mgh.harvard.edu/>), FsFast (<https://surfer.nmr.mgh.harvard.edu/fswiki/FsFast/>), and custom Matlab code. Images were motion corrected (time points where the difference in total vector motion from the previous time point exceeded 1mm were excluded, and orthogonalized motion measures were used as nuisance regressors for the GLM), detrended, and fit using a standard gamma function ($d = 2.25$ and $t = 1.25$). Age 8 data were also distortion-corrected using the field maps every two runs.

fROI definition. We used a watershed GSS method^{41,42} to define a VWFA parcel as a search-space for the VWFA fROIs, from a separate group of adults who participated in exactly the same fMRI experiment. These parcels were registered to each child's native brain anatomy at age 8 using the inverse transform of Freesurfer's CVS toolbox^{43,44} (https://surfer.nmr.mgh.harvard.edu/fswiki/mri_cvs_register) to the CVS average-35 template. Each child's contrast map for the even-runs was thresholded at $P < 0.005$. Individual-subject fROIs were constructed from the intersection of the relevant parcel (for IFFA, VWFA, and IPFS separately) and the contrast map for the even runs (thresholded and not spatially smoothed). Contrast maps for line drawings of faces > line drawings of objects defined IFFA, words > object line drawings defined VWFA, and object line drawings > Scrambled words defined IPFS. These fROIs did not overlap in 7 of 14 children and had minimal overlap in the remaining children ($2.84 \pm 0.83\%$ of the IFFA and VWFA fROIs overlapped and $2.87 \pm 0.36\%$ of the IFFA, VWFA, and IPFS overlapped). We removed any overlapping voxels between these fROIs, thus creating non-overlapping VWFA, IFFA, and IPFS fROIs in each individual's native anatomy. We used these non-overlapping fROIs for all further analyses. The odd runs (also not spatially smoothed) were then used for calculating PSC for each stimulus category.

Motion measures. Total vector motion and root mean squared rotation were calculated using FSFast. Time-points that had more than 1mm total vector motion from the previous time-point were removed. We chose the best four runs of fMRI data for each subject as those with the fewest time-points removed. After removing time-points for the best four runs, we averaged the measures of motion across runs for each subject. We also extracted motion measures from DWI data using TRACULA software⁴⁵: average translation, rotation, percentage bad slices, and average drop-out score (for slices with excessive intensity drop-out).

We found that none of the fMRI motion measures was correlated with any of the DWI motion measures (at $P < 0.05$; **Supplementary Table 3**).

Longitudinal registration of age 5 to age 8 data. We registered the age 5 anatomical data of each subject to the same subject's age 8 anatomical data using Advanced Normalization Tools (ANTs version 2.1.0; <http://stnava.github.io/ANTs/>) registration^{46,47}. ANTs has been previously used for lifespan analyses of brain morphology⁴⁸ and function⁴⁹ in both adult⁴⁸ and pediatric brain data^{49–51} including infants⁵². We transformed the age 8 brain to the age 5 brain using the symmetric normalization toolbox with Gaussian regularization and initialized the transform with the affine registration matrix from Freesurfer's `mri_robust_register` software^{53–55} (https://surfer.nmr.mgh.harvard.edu/fswiki/mri_robust_register).

We calculated the accuracy of the ANTs longitudinal registration for two structures: the large VWFA parcel, which we used as a search space to define the VWFA fROI for each subject, and the left occipitotemporal cortex region (IOTC, which is derived from combining the left fusiform and left inferior temporal gyrus from the Freesurfer parcellation; this region is important because we used it as a seed for tractography, explained below). We mapped either the VWFA parcel or the IOTC from age 8 to the age 5 anatomy using ANTs and calculated the overlap between this ANTs-registered region with the region defined by direct registration to the age 5 data (that is, age 8 to age 5 registered region versus region registered directly to age 5). This procedure quantified error due to longitudinal registration. We used two measures of accuracy: the overlap coefficient and modified Hausdorff. The overlap coefficient is the size of the intersection of the two regions divided by the minimum size of the two regions. The modified Hausdorff⁴⁵ is defined as the minimum distance of each voxel in one region from the other region, averaged over all voxels in the two regions (that is, average distance from the age 8-to-age 5 registered region to the native age 5 region); this measure indicates that all points in the registered region are on average 'X' far from the native age 5 region. The overlap coefficient for the IOTC was 0.8700 ± 0.0063 and 0.8731 ± 0.0084 for the VWFA parcel; the modified Hausdorff metric was 0.1471 ± 0.0133 voxels for the IOTC anatomical region, and 0.1437 ± 0.0142 voxels for the VWFA parcel.

Comparison of the VWFA's selectivity to letters and words. The fMRI data at age 5 had slightly different stimulus conditions than the fMRI data acquired at age 8: age 5 data included letters instead of words and did not include an 'Objects' condition. To test whether the VWFA responds selectively not only to words but also to individual letters, we performed several experiments in a cohort of adults: the VWFA localizer that is, 'age 8 fMRI experiment', and a version of the VWFA localizer that included individual letters in addition to the other four categories (line drawings of objects, line drawings of faces, words and scrambled words). The VWFA localizer (that is, age 8 fMRI experiment) was collected in another scan session and we used that scan session to define the VWFA, IFFA, and IPFS in exactly the same way that we defined them for children. We compared letter versus word selectivity in each of these regions. We compared VWFA letter selectivity and word selectivity versus selectivities to the other categories in adults. The VWFA showed a significant interaction by condition (repeated measures ANOVA by condition: $F_4 = 22.26$, $P = 1.76 \times 10^{-5}$). The response to letters and words in the VWFA did not differ significantly ($T = 0.16$, $P = 0.885$) and each of these conditions produced a significantly higher response than the object condition (letters versus objects: $T = 5.66$, $P = 1.09 \times 10^{-2}$; words versus objects: $T = 9.27$, $P = 2.66 \times 10^{-3}$). The IFFA and IPFS showed higher responses to faces and objects, respectively, over any other category, including words and letters (IFFA: ANOVA interaction: $F_4 = 31.86$, $P = 2.63 \times 10^{-6}$; faces versus words, letters: $T = 4.20$, $P = 2.46 \times 10^{-2}$; $T = 8.10$, $P = 3.93 \times 10^{-3}$; IPFS: $F_4 = 11.50$, $P = 4.53 \times 10^{-4}$; objects versus words, letters: $T = 3.76$, $P = 3.30 \times 10^{-2}$; $T = 3.60$, $P = 3.68 \times 10^{-2}$). These analyses confirm that the VWFA shows no difference in the response to words versus individual letters, with both conditions significantly higher than to objects. Thus, if the VWFA was selective to orthography at age 5, we would have expected to find comparable selectivity to letters at age 5 as we observed for words at age 8.

DWI image acquisition. The diffusion-weighted scan in kindergarten (5 min total) included 10 non-diffusion weighted volumes ($b = 0$) and 30 diffusion-weighted volumes (that is, 30 diffusion directions) acquired with non-collinear gradient directions ($b = 700$ s/mm²), all at 128×128 base resolution and isotropic voxel resolution of 2.0 mm³. Diffusion weighted images were checked for motion artifact and processed using FSL's FDT software (<http://fsl.fmrib.ox.ac.uk/fsl/fslwiki/FDT/>)⁵⁶.

The diffusion-weighted scan at age 8 was identical to the kindergarten scan except that it included 60 diffusion-weighted volumes ($b = 700$ s/mm²) because the children could stay motionless in the scanner for longer periods of time. Children watched a movie of their choice during the anatomical and DWI scanning.

DWI longitudinal prediction analysis. We registered the age 5 Freesurfer segmentation and parcellation results (`aparc+aseg`) to each individual's age 5 diffusion images using Freesurfer's `bbregister` function⁵⁷, which uses surface-based algorithms to register images, and we initialized the registration with FSL's FLIRT. We combined the DWI-registered left fusiform and left inferior temporal gyrus parcels into one seed region (left occipitotemporal seed region; IOTC). Each voxel within this region was used as a seed and the remaining 81 parcels were used as target regions for fiber tracking. The principal diffusion directions were calculated per voxel, and probabilistic diffusion tractography was carried out using FSL-FDT⁵⁶ with 10,000 streamline samples in each seed voxel to create a connectivity distribution to each of the target regions, while avoiding a mask consisting of the ventricles. Thus, every voxel within the IOTC seed region was described by a vector of connection probabilities to each other brain region.

Each participant's age 8 functional image (t -statistic) for the contrast of Words > Objects from either the best 4 runs (assessed by least motion) or even runs (for split-half reliability measurements) was registered to his or her structural image at age 5 using the longitudinal registration approach described above, and the resulting registered functional image was then registered to the age 5 DWI data using Freesurfer's `bbregister` and initialized using FSL's FLIRT. Thus, every voxel was also described by a vector of t statistics for each functional contrast.

To predict function from connectivity, we used the methods described in refs. 1,2. Briefly, we used a leave-one-subject-out cross-validation (LOOCV) routine⁵⁸, where a single subject's data was excluded, trained a model with all of the remaining subjects' voxel-wise data, and then applied the model to the left-out subject. This routine was repeated for all subjects, generating independent predictions. Each voxel of the seed parcel was paired with its connectivity vector to every other brain region, its spatial coordinates, and its word-selectivity (response to words > objects). We used in-house MATLAB code (R2011b; The Mathworks) and the LibSVM toolbox (<http://www.csie.ntu.edu.tw/~cjlin/libsvm/>) for these analyses. We concatenated all of the native-space voxels from each subject's IOTC seed region (excluding all voxels of the left-out subject) and trained an SVR model with kernel = radial basis function, $\gamma = 0.012$ ($1/\text{number of features}$), $\epsilon = 0.1$) on the standardized and linearized word-selectivity and connectivity vector of that voxel. Thus each voxel was an independent observation in the regression model. Because all analyses were performed on subject-specific anatomy, the number of voxels in the seed varied among individuals, but the model was blind to the participant each voxel belonged to. We applied this model to the DWI data of the subject that we left out of the analysis, resulting in a predicted fMRI value for word-selectivity for every voxel of the IOTC seed region. To evaluate the accuracy of the predictions, we performed Pearson's correlations on the predicted versus actual fMRI responses for each individual and Fisher z -transformed the resulting correlation coefficients. These prediction accuracies were tested against random permutations and other benchmarks (below).

Random permutations. We used the same data matrices that were used for DWI predictions but here we shuffled the pairings between the fMRI responses and DWI connectivity vectors. We shuffled these 5,000 times, generating 5,000 predictions from randomly shuffled data for each subject, and performed a permutation test (exact test) of each subject's z -transformed correlation coefficient for DWI predictions against the distribution of correlation coefficients from the permutations.

Group-average prediction analysis. We compared the accuracy of the DWI predictions with a group analysis model (see refs. 1,2). The group models were also made through LOOCV. Each participant's functional data at age 8 were spatially normalized into CVS average 35 template space with Freesurfer's CVS registration and superimposed to create composite maps. We performed a least-squares random-effects test on all but one participant using Freesurfer's `FsFast`. The resulting t statistic image, which was based on all the other participants in normalized CVS space (**Supplementary Fig. 5**), was then mapped to the native age 5 anatomy of the participant left out of the group analysis (using the reverse

CVS normalization transform from age 5 to group template space). We again correlated the actual versus predicted fMRI values within the IOTC seed mask, Fisher z -transformed the resulting coefficients, and performed a paired t test to compare DWI prediction accuracies to group prediction accuracies.

Subject-to-subject prediction analysis. We mapped each child's anatomical data at age 8 to each other child's anatomical data at age 5 using ANTS software (see above). We used Freesurfer's `bbregister` function to map the fMRI data at age 8 to the anatomical data at age 5, and then mapped the registered fMRI data to every other child's anatomy (using the registration matrix from ANTS software). We then registered that data to the DWI data using `bbregister`. This process of registering each child's fMRI data at age 8 to each other child's DWI data at age 5 generated voxel-wise predictions for each subject based on each other's child's data.

Split-half reliability. We also compared the DWI predictions to 'ceiling predictions' or predictions of age 8 word selectivity from left-out age 8 fMRI runs. We divided the residual sum of squares for the DWI predictions by the total sum of squares for the split-half reliability to calculate the normalized (R^2). This measurement represents the best possible predictions of functional selectivity for each subject because they are based on the same subject's own fMRI data. It also captures the reliability of the fMRI data, and can therefore be used to normalize the DWI prediction accuracies and assess how much of the reliable variance (R^2) in age 8 word-selectivity can be predicted from age 5 DWI data.

Overlap measurements. We generated an fROI from the DWI predictions by masking the DWI predicted fMRI responses with the larger VWFA GSS parcel (see above) and thresholded the DWI predictions at > 0.4 s.u. (same threshold as Fig. 3) as well as upper bound (>0.8 s.u.) and lower bound (>0.2 s.u.). We generated the actual fROIs using the same criteria. We also generated fROIs from the split-half fMRI data in exactly the same manner. We compared the DWI predicted fROIs (and the split-half predicted fROIs) to the actual fROIs for each subject using the same two measures as described above (overlap coefficient and modified Hausdorff metric).

fROI-based DWI tractography analysis. The VWFA, IFFA, and IPFS were used as seed regions for fiber tracking for each individual; the remaining 81 individual-subject parcels from the Freesurfer segmentation were similarly DWI-registered, and used as the target regions for tractography (we excluded the fusiform and inferior temporal gyrus as targets because the voxels within VWFA, IFFA, and/or IPFS landed somewhere within these regions and it would be redundant to include a region as both a seed and a target). Tractography was run from each seed fROI to each target parcel (and back) and averaged the connectivity values to and from the fROIs. We performed a two-way ANOVA to compare IFFA, VWFA, and IPFS connectivity to the 81 target regions. We also performed separate two-way ANOVAs to compare the VWFA to the IFFA and IPFS separately, and *post hoc* t tests were performed if we observed a significant fROI \times target interaction.

Statistics. We used a within-subject design in these experiments; therefore, there was no experimental group randomization or blinding. We followed standard procedures in the field and statistical procedures in line with previously published studies^{1,2,57}. All Student's t tests are paired and two-tailed; F tests in ANOVAs and exact permutation tests were one-tailed, as is standard for such comparisons. Data distribution was assumed to be normal, but this was not formally tested. No statistical methods were used to pre-determine sample sizes but our sample sizes are similar to those reported in previously published longitudinal studies in children or fMRI studies on decoding and prediction within subject (for example, see refs. 59,60).

Data availability. The data that support the findings of this study are available from the corresponding author upon request.

A **Supplementary Methods Checklist** is available.

30. Woodcock, R.W. *Woodcock Reading Mastery Tests, Revised, Examiner's Manual* (American Guidance Service, 1998).
31. Kaufman, A.S. & Kaufman, N.L. *Kaufman Brief Intelligence Test* (Wiley Online Library, 2004).
32. Dunn, D.M. & Dunn, L.M. *Peabody Picture Vocabulary Test: Manual* (Pearson, 2007).
33. van der Kouwe, A.J.W., Benner, T., Salat, D.H. & Fischl, B. Brain morphometry with multiecho MPRAGE. *Neuroimage* **40**, 559–569 (2008).
34. Tisdall, M.D. *et al.* Volumetric navigators for prospective motion correction and selective reacquisition in neuroanatomical MRI. *Magn. Reson. Med.* **68**, 389–399 (2012).
35. Dale, A.M., Fischl, B. & Sereno, M.I. Cortical surface-based analysis. I. Segmentation and surface reconstruction. *Neuroimage* **9**, 179–194 (1999).
36. Fischl, B. *et al.* Whole brain segmentation: automated labeling of neuroanatomical structures in the human brain. *Neuron* **33**, 341–355 (2002).
37. Fischl, B. *et al.* Automatically parcellating the human cerebral cortex. *Cereb. Cortex* **14**, 11–22 (2004).
38. Desikan, R.S. *et al.* An automated labeling system for subdividing the human cerebral cortex on MRI scans into gyral based regions of interest. *Neuroimage* **31**, 968–980 (2006).
39. Thesen, S., Heid, O., Mueller, E. & Schad, L.R. Prospective acquisition correction for head motion with image-based tracking for real-time fMRI. *Magn. Reson. Med.* **44**, 457–465 (2000).
40. Gorgolewski, K. *et al.* Nipype: a flexible, lightweight and extensible neuroimaging data processing framework in python. *Front. Neuroinform.* **5**, 13 (2011).
41. Fedorenko, E., Hsieh, P.-J., Nieto-Castañón, A., Whitfield-Gabrieli, S. & Kanwisher, N. New method for fMRI investigations of language: defining ROIs functionally in individual subjects. *J. Neurophysiol.* **104**, 1177–1194 (2010).
42. Julian, J.B., Fedorenko, E., Webster, J. & Kanwisher, N. An algorithmic method for functionally defining regions of interest in the ventral visual pathway. *Neuroimage* **60**, 2357–2364 (2012).
43. Postelnicu, G., Zöllei, L. & Fischl, B. Combined volumetric and surface registration. *IEEE Trans. Med. Imaging* **28**, 508–522 (2009).
44. Zöllei, L., Stevens, A., Huber, K., Kakunoori, S. & Fischl, B. Improved tractography alignment using combined volumetric and surface registration. *Neuroimage* **51**, 206–213 (2010).
45. Yendiki, A. *et al.* Automated probabilistic reconstruction of white-matter pathways in health and disease using an atlas of the underlying anatomy. *Front. Neuroinform.* **5**, 23 (2011).
46. Wang, H. & Yushkevich, P.A. Multi-atlas segmentation with joint label fusion and corrective learning—an open source implementation. *Front. Neuroinform.* **7**, 27 (2013).
47. Menze, B.H. *et al.* The Multimodal Brain Tumor Image Segmentation Benchmark (BRATS). *IEEE Trans. Med. Imaging* **34**, 1993–2024 (2015).
48. Tustison, N.J. *et al.* Large-scale evaluation of ANTs and FreeSurfer cortical thickness measurements. *Neuroimage* **99**, 166–179 (2014).
49. Avants, B.B. *et al.* The Insight Toolkit image registration framework. *Front. Neuroinform.* **8**, 44 (2014).
50. Jain, V. *et al.* Longitudinal reproducibility and accuracy of pseudo-continuous arterial spin-labeled perfusion MR imaging in typically developing children. *Radiology* **263**, 527–536 (2012).
51. Lawson, G.M., Duda, J.T., Avants, B.B., Wu, J. & Farah, M.J. Associations between children's socioeconomic status and prefrontal cortical thickness. *Dev. Sci.* **16**, 641–652 (2013).
52. Pineda, R.G. *et al.* Alterations in brain structure and neurodevelopmental outcome in preterm infants hospitalized in different neonatal intensive care unit environments. *J. Pediatr.* **164**, 52–60 (2014).
53. Reuter, M., Rosas, H.D. & Fischl, B. Highly accurate inverse consistent registration: a robust approach. *Neuroimage* **53**, 1181–1196 (2010).
54. Reuter, M. & Fischl, B. Avoiding asymmetry-induced bias in longitudinal image processing. *Neuroimage* **57**, 19–21 (2011).
55. Reuter, M., Schmansky, N.J., Rosas, H.D. & Fischl, B. Within-subject template estimation for unbiased longitudinal image analysis. *Neuroimage* **61**, 1402–1418 (2012).
56. Behrens, T.E.J., Berg, H.J., Jbabdi, S., Rushworth, M.F.S. & Woolrich, M.W. Probabilistic diffusion tractography with multiple fibre orientations: What can we gain? *Neuroimage* **34**, 144–155 (2007).
57. Greve, D.N. & Fischl, B. Accurate and robust brain image alignment using boundary-based registration. *Neuroimage* **48**, 63–72 (2009).
58. Hastie, T., Tibshirani, R. & Friedman, J. *The Elements of Statistical Learning: Data Mining, Inference, and Prediction* (Springer, 2009).
59. Huth, A.G., de Heer, W.A., Griffiths, T.L., Theunissen, F.E. & Gallant, J.L. Natural speech reveals the semantic maps that tile human cerebral cortex. *Nature* **532**, 453–458 (2016).
60. Finn, A.S., Sheridan, M.A., Kam, C.L.H., Hinshaw, S. & D'Esposito, M. Longitudinal evidence for functional specialization of the neural circuit supporting working memory in the human brain. *J. Neurosci.* **30**, 11062–11067 (2010).